Earth and Planetary Science Letters 304 (2011) 71–84

Contents lists available at ScienceDirect

Earth and Planetary Science Letters

journal homepage: www.elsevier.com/locate/epsl

Seismic velocities, anisotropy and deformation in Siberian cratonic mantle: EBSD data on xenoliths from the Udachnaya kimberlite

Jérôme Bascou [a,*], Luc S. Doucet [a], Sylvaine Saumet [a,1], Dmitri A. Ionov [a], Igor V. Ashchepkov [b], Alexander V. Golovin [b]

[a] Université de Lyon, Université Jean Monnet, 42023 Saint Etienne and UMR-CNRS 6524, Laboratoire Magmas et Volcans, France
[b] Institute of Geology and Mineralogy SD RAS, Novosibirsk 630090, Russia

ARTICLE INFO

Article history:
Received 5 August 2010
Received in revised form 17 December 2010
Accepted 16 January 2011
Available online 23 February 2011

Editor: L. Stixrude

Keywords:
Cratonic mantle
Deformation
Crystal preferred orientation
Anisotropy
Microstructure

ABSTRACT

The study presents microstructures and crystallographic preferred orientations (CPO) of minerals obtained by electron back-scattered diffraction (EBSD) in a suite of 23 fresh mantle xenoliths (20 peridotites, 2 eclogites and 1 pyroxenite) from the Udachnaya kimberlite in central Siberian craton. The suite includes coarse spinel- and garnet-facies peridotites equilibrated at 760–1000 °C from the upper part of the mantle lithosphere (45–160 km) and porphyroclastic garnet peridotites from the base of the lithosphere (160–210 km; 1200–1320 °C). The data indicate that dislocation creep is the main deformation mechanism in the peridotites and eclogites. The CPO patterns of olivine suggest a dominant activation of the (010) [100] slip system. Within this general pattern, coarse peridotites show a better alignment of [100]-olivine while porphyroclastic rocks have a better alignment of [010]-olivine. Recrystallization in the porphyroclastic peridotites reduces olivine grain size and facilitates the development of a mosaic matrix that leads to a decrease in the CPO strength. Orthopyroxene in peridotites slips parallel to (100) [001]; clinopyroxene shows a clear slip direction on [001] in both peridotites and eclogites. Seismic properties estimated from the CPO data and modal abundances of major minerals show significant differences between peridotites, eclogites and pyroxenites; some differences also exist between peridotite types. Importantly, coarse peridotites have much higher anisotropy than eclogites and may yield higher P-wave velocities in the fast direction ($V_p \geq 8.8$ km/s). Thus, the extremely high sub-Moho velocities ($V_p > 8.7$ km/s) reported from some seismic profiles in the Siberian craton can be better explained by strong anisotropy of coarse peridotites in a horizontally foliated mantle rather than by the presence of abundant eclogites.

1. Introduction

Cratons are the oldest and thickest domains of the earth's lithosphere. They make up ~40% of exposed continental regions and may have 'roots' as deep as 300–400 km. Deep cratonic rocks have particular petrologic and chemical signatures; cratonic mantle is generally very refractory (e.g. higher Mg#), with common garnet-bearing and sheared rocks (Jordan, 1975). Fragments of deep cratonic lithosphere are brought up by kimberlitic magmas, but such xenoliths are usually altered, with major minerals, like olivine and orthopyroxene (opx), completely or partially replaced by secondary materials (Pearson and Wittig, 2008). As a result, some petrophysical properties of cratonic mantle and their relation to petrologic and chemical features and deformation remain poorly constrained.

Cratons are made of juxtaposed domains with different modal and chemical compositions and microstructures (e.g., Artemieva, 2009; Griffin et al.; 1999; Ionov et al., 2005; Kendall et al., 2002). Their complex structure hinders interpretation of geophysical data on a regional scale. While large amounts of seismic data have been obtained in Siberia from Peaceful Nuclear Explosion profiles (e.g., Egorkin et al., 1987a; Nielsen et al., 1999; Nielsen et al., 2002; Pavlenkova and Pavlenkova, 2006; Yegorkin and Pavlenkova, 1981), Chemical Explosion profiles (e.g., Suvorov et al., 2006), and passive surface wave tomography and SKS splitting studies (Oreshin et al., 2002), anomalously high P-wave velocities (>8.6 km/s) detected in the uppermost mantle around kimberlite fields (Suvorov et al., 2006; Uarov, 1981) have not been adequately explained as yet.

A recent study by Kobussen et al. (2006) reported laboratory seismic measurements on 2 eclogite and 3 fresh peridotite xenoliths from Udachnaya in central Siberian craton. The P-wave velocities measured in their study are usually lower than 8.5 km/s (rarely reaching 8.6 km/s) and thus not high enough to explain the V_p

* Corresponding author at: Université de Lyon, Université Jean Monnet, 42023, Saint Etienne, France. Tel.: +33 477485124; fax: +33 477485108.
E-mail address: jerome.bascou@univ-st-etienne.fr (J. Bascou).
[1] Now at Institut de Physique du Globe de Paris, 4 place Jussieu, Case 89, 75005 Paris, France.

0012-821X/$ – see front matter © 2011 Elsevier B.V. All rights reserved.
doi:10.1016/j.epsl.2011.01.016

anomalies recorded in field studies. Seismic velocities were also calculated by Kobussen et al. (2006) based on optical measurements of crystallographic preferred orientation (CPO) obtained from universal stage for 100 olivine grains in each of two sheared and one coarse garnet peridotites. The results suggest that some refractory peridotites could match natural V_p anomalies, but this inference is equivocal considering the small number of samples, the limited range of peridotite types and the measurement of only olivine.

High seismic velocities (up to 8.6 km/s) calculated from CPO data on major minerals were reported for peridotite xenoliths in Cenozoic basalts at Tokinsky Stanovik (Tok) in SE Siberia (Tommasi et al., 2008). However, the Tok xenoliths differ in modal and chemical composition from kimberlite-hosted peridotites in central Siberian craton. The Tok xenoliths represent shallow (40–60 km) spinel facies mantle on the margin of the craton where the deep lithosphere may have been removed, and the remaining lithospheric mantle was percolated by basaltic melts to produce enrichments in iron and clinopyroxene (cpx) (Ionov et al., 2005; Ionov et al., 2006). Hence, the data on the Tok suite may not be directly relevant to petrophysical properties of typical cratonic mantle in Siberia.

Advances in Electron Back-Scattered Diffraction (EBSD) methods enable to detect minor variations in CPO patterns of ultramafic rocks related to equilibration temperature (T) and pressure (P), deformation, recrystallization, modal and chemical variations (Bascou et al., 2008; Holtzman et al., 2003; Jung and Karato, 2001; Mainprice et al., 2005, Tommasi et al., 2004; Tommasi et al., 2006; Vauchez and Garrido, 2001; Vauchez et al., 2005; Vonlanthen et al., 2006). Importantly, the recent work has shown that variations in fabric patterns of rock-forming minerals may be responsible for differences in seismic properties.

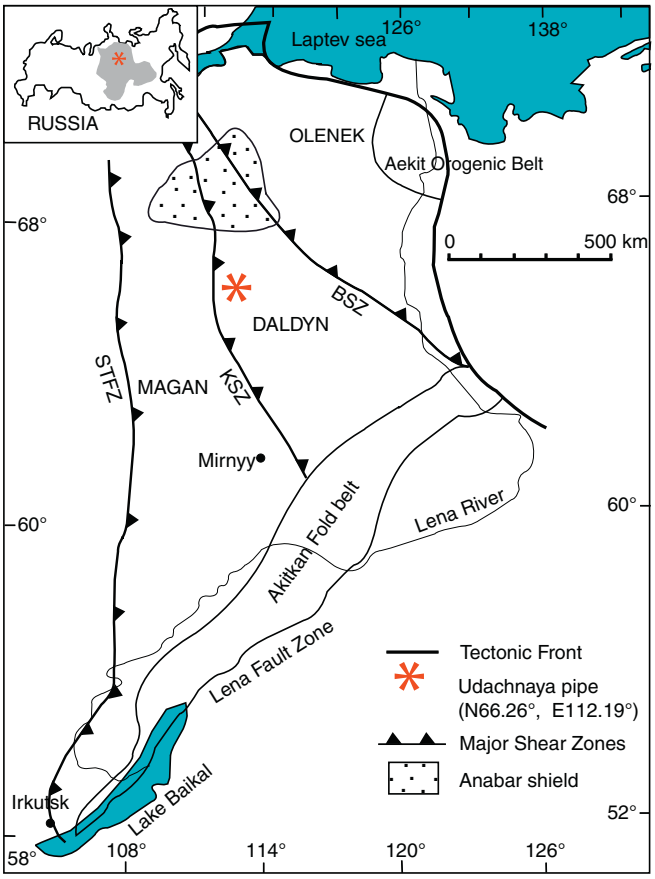

Fig. 1. Locality map for the Udachnaya kimberlite pipe. Inset shows the Siberian Craton in gray on the outline map of Russia. Also shown are major shear zones that delineate the north–south boundaries of main tectonic provinces (Magan, Daldyn and Olenek); STFZ: Sayano-Taymyr Fault Zone; KSZ: Kotuykan Shear Zone; BSZ: Billyakh Shear Zone after Griffin et al. (1999) and Rosen et al. (1994).

This paper presents microstructural and CPO data on a suite of unusually fresh xenoliths (20 peridotites, 2 eclogites, and 1 pyroxenite) from the Udachnaya kimberlite in central Siberia. We use the data to determine seismic properties and explain observations, like high velocities in the shallow mantle of the Siberian craton; we also seek to assess relationships between deformation, modal and chemical compositions, and seismic properties of cratonic mantle.

2. The Udachnaya xenolith suite

2.1. Geological setting and samples

The xenoliths were collected deep in the open-pit diamond mine at the ~350 Ma old (Davis et al., 1980; Kinny et al., 1997) Udachnaya-East kimberlite in the Daldyn region of central Siberia limited by major shear zones (Fig. 1). Oldest crustal ages in the Siberian craton are >3 Ga; its amalgamation was completed ~1.9 Ga ago (Rosen et al., 1994).

The xenoliths in this study represent all major rock types reported previously from Udachnaya (Boyd et al., 1997; Ionov et al., 2010; Sobolev, 1990). They are exceptionally fresh for cratonic xenoliths (loss on ignition from −1% to +0.5%) and contain essentially unaltered olivine and opx. The samples are listed in Table 1, which also gives their modal compositions (calculated from bulk-rock and mineral compositions) and Mg# of olivine [$Mg\#_{ol} = Mg/(Mg+Fe)_{at}$]. The modal and chemical data for the peridotites are after Ionov et al. (2010). Modal abundances were also estimated from EBSD maps obtained by automatic measurements with sampling steps from 50 to 100 μm; the EBSD-based values are similar to those reported by Ionov et al. (2010).

2.2. Rock types and microstructures

The peridotites are garnet and spinel facies rocks grouped into coarse (granular) and porphyroclastic textural types (Fig. 2a–e).

Coarse peridotites (Fig. 2a–b) are medium- to coarse-grained rocks with protogranular to mosaic equigranular microstructures. Olivine and opx do not show intra-crystalline evidence of deformation such as subgrains; they commonly have similar grain size (1–5 mm) and equant shapes but opx also occurs as lobate grains that may embay olivine, and some opx have thin exolution lamellae. Cpx (1–6%) occurs interstitially or as small anhedral grains in the vicinity of opx. Nine coarse peridotites are spinel facies rocks: eight harzburgites (1–4% cpx) and one wehrlite. Spinel (≤1%) is anhedral and usually forms interstitial segregations between grains of silicates or intergrowths with opx (Fig. 2a). U15 has a clear shape-preferred orientation of large olivine grains; U52 shows an alignment of spinel grains. Coarse garnet peridotites may contain some spinel; three out of four are harzburgites (1–4% cpx), one is low-cpx (6%) lherzolite. Garnet (1–4%) mainly forms large (several mm) equant grains or irregular aggregates (Fig. 2b).

Porphyroclastic peridotites (Fig. 2c–e) contain two types of olivine and opx: large (2–4 mm) porphyroclasts and a medium- to fine-grained matrix of recrystallized grains (neoblasts). All display foliation defined by grain elongation; xenoliths U71, U50A and U70A also show lineation. The porphyroclasts show undulose extinction and closely spaced subgrain boundaries, i.e. clear evidence of plastic deformation. Two types of porphyroclastic samples can be distinguished from matrix observation. In the first type (U71, U50A, and U9D), the matrix encloses both small, deformation-free polygonal neoblasts (<0.5 mm) and larger anhedral neoblasts, which display internal strain features. In the second type of porphyroclastic samples (U70A, U57A, U267, and U183A), the matrix is mainly constituted of very fine (1–200 μm), euhedral, optically strain-free neoblasts, i.e. the matrix has a mosaic microstructure (e.g., Boyd et al., 1997). Three porphyroclastic rocks in this study are harzburgites (1–4% cpx), four

Table 1
Seismic properties of xenolith samples.

Samples	Mg# (ol)	Modal abundance (wt.%)				V_{pmax}	V_{pmin} (km/s)	Vp_{ave}	AVp (%)	Vs_{1max}	Vs_{1min} (km/s)	Vs_{2max}	Vs_{2min}	Vs_{ave} (km/s)	AVs_{max} (%)	J_{index}	Density (g/cm^3)
Coarse spinel peridotites																	
		ol	opx	cpx	spl											*ol*	
U504	92.8	84	13	2	1	9.02	8.04	8.53	11.50	5.10	4.89	4.92	4.63	4.89	8.01	5.72	3.31
U15	92.8	65	31	4	1	8.60	7.97	8.29	7.60	5.00	4.86	4.89	4.65	4.85	6.32	11.00	3.31
U52	92.8	68	28	3	1	8.58	7.99	8.29	7.10	4.97	4.86	4.89	4.66	4.85	5.72	5.85	3.31
U1109	92.8	*92*	*6*	*1*	*1*	8.74	8.13	8.44	7.30	4.99	4.90	4.93	4.71	4.88	5.92	5.21	3.32
UV93/3	92.2	*96*	*2*	*1*	*1*	8.65	8.18	8.42	5.60	4.97	4.87	4.90	4.72	4.87	4.93	6.72	3.33
UV101/03	92.9	*82*	*14*	*3*	*1*	8.62	8.17	8.40	5.50	4.98	4.87	4.89	4.71	4.86	4.85	4.24	3.31
UV504/09	92.8	*88*	*10*	*1*	*1*	8.77	8.05	8.41	8.60	5.09	4.81	4.89	4.74	4.88	6.56	7.06	3.32
UV590/09	92.8	*88*	*10*	*1*	*1*	8.61	8.11	8.36	6.00	4.99	4.84	4.88	4.74	4.86	4.94	3.83	3.32
U225A	90.3	86	*1*	*12*	*1*	8.81	8.07	8.44	8.70	4.94	4.85	4.87	4.60	4.82	6.00	3.56	3.38
Average						*8.71*	*8.08*	*8.40*	*7.54*	*5.00*	*4.86*	*4.90*	*4.68*	*4.86*	*5.92*	*5.91*	*3.32*
Coarse garnet peridotites																	
		ol	opx	cpx	gar											*ol*	
U29-2	92.2	69	22	6	3	8.48	8.11	8.30	4.40	4.92	4.85	4.86	4.74	4.84	3.54	4.08	3.32
U506B	92.5	77	16	3	4	8.70	8.13	8.42	6.80	4.98	4.87	4.89	4.70	4.86	4.66	4.78	3.33
U280B	91.9	85	9	2	4	8.61	8.20	8.41	4.90	4.95	4.85	4.91	4.73	4.86	4.13	4.11	3.34
U260B	91.7	90	5	4	1	8.85	8.09	8.47	9.00	5.03	4.89	4.92	4.65	4.87	6.79	5.74	3.33
Average						*8.66*	*8.13*	*8.40*	*6.28*	*4.97*	*4.87*	*4.90*	*4.71*	*4.86*	*4.78*	*4.68*	*3.33*
Porphyroclastic garnet peridotites																	
		ol	opx	cpx	gar											*ol*	
U71	91.2	77	11	5	7	8.64	8.01	8.33	7.50	5.01	4.80	4.84	4.72	4.84	5.45	7.04	3.36
U50A	91.0	65	22	6	7	8.45	8.06	8.26	4.80	4.93	4.81	4.84	4.74	4.83	3.64	3.21	3.35
U9D	90.5	70	24	1	5	8.61	7.99	8.30	7.50	4.97	4.85	4.86	4.67	4.84	5.84	8.07	3.35
U70A	90.1	79	10	6	5	8.62	8.05	8.34	6.90	4.96	4.82	4.85	4.68	4.83	5.21	–	3.36
U57A	91.1	85	9	4	2	8.62	8.03	8.33	7.10	4.99	4.80	4.85	4.72	4.84	5.32	2.93	3.33
U267	89.0	53	22	12	13	8.36	8.13	8.25	2.80	4.88	4.78	4.82	4.74	4.81	2.62	2.22	3.39
U183A	91.5	81	13	2	4	8.44	8.19	8.32	2.90	4.91	4.84	4.87	4.79	4.85	2.41	3.28	3.34
Average						*8.52*	*8.07*	*8.29*	*5.43*	*4.95*	*4.81*	*4.85*	*4.73*	*4.83*	*4.21*	*4.46*	*3.35*
Eclogite																	
		gar	omph													*omph*	
UV-73-03		*60*	*40*			8.71	8.60	8.66	1.30	4.98	4.92	4.96	4.90	4.94	1.40	10.58	3.65
UV-KC-147		*57*	*43*			8.75	8.53	8.64	2.50	4.99	4.92	4.96	4.88	4.94	1.78	11.97	3.64
Average						*8.73*	*8.57*	*8.65*	*1.90*	4.99	4.92	4.96	4.89	4.94	1.59	*11.27*	3.64
Orthopyroxenite																	
		opx	cpx	ol													
UV-KC-44/08		*86*	*9*	*5*		7.95	7.78	7.87	2.20	4.81	4.73	4.77	4.69	4.75	2.07	–	3.28

Modal estimates were obtained by least squares method from whole-rock and minerals analyses (Ionov et al., 2010).
Modal estimates in italic were obtained from EBSD map analyses. [Mg#Ol = Mg/(Mg + Fe)$_{at}$].
AVp and AVs: anisotropy of P- and S-waves; Vp_{ave} and Vs_{ave}: average of seismic velocities.

are lherzolites (5–12% cpx); all contain garnet (2–13%) as equant or elongated grains a few mm in size.

Eclogites are made up of equant garnet (60%) and cpx (40%) 3–5 mm in size, and accessory rutile and sulfide (<2%). Large cpx show undulose extinction and are usually altered. Garnet commonly has kelyphite rims. *Pyroxenite* UV-KC-44/08 has 86% opx, 9% cpx and 5% olivine. The pyroxene grains (up to 1 cm) show straight and irregular boundaries; olivine shows no deformation evidence.

2.3. Olivine composition, P-T and modal estimates

Compositional variations, particularly of Mg and Fe contents in olivine, induce changes in seismic properties of peridotites (e.g., Tommasi et al., 2004). In the studied samples, Mg#$_{ol}$ ranges from 0.890 to 0.929, with the lowest values for porphyroclastic rocks and wehrlite U225A, and the highest for coarse spinel peridotites (Table 1). There are no significant differences between cores and rims of coarse olivine or between porphyroclasts and neoblasts (see also Sobolev et al., 2009).

P-T estimates (Ionov et al., 2010) were obtained using the Ca-opx thermometer of Brey and Kohler (1990) and the cpx–opx thermometer of Taylor (1998) in combination with the opx-garnet barometer of Nickel and Green (1985). Coarse garnet peridotites equilibrated at 870–1000 °C and 2.5–5.5 GPa plot close to the 40 mW/m^2 geotherm of Pollack and Chapman (1977) (Fig. 3). Their T range partly overlaps the T range for spinel peridotites (760–965 °C, calculated with P = 2.5 GPa) indicating that coarse garnet and spinel peridotites coexist at P = 2.5–5 GPa. Porphyroclastic rocks yield higher P values (5.4 to 6.6 GPa) and plot above the 40 mW/m^2 geotherm, likely due to heating shortly before transport to the surface.

Modal compositions are illustrated on an olivine–opx–cpx triangular diagram (Fig. 4). The porphyroclastic rocks have higher modal cpx than the coarse peridotites, which may be due to higher degrees of modal metasomatism (refertilization) (Boyd et al., 1997; Ionov et al., 2010).

3. Texture and calculated seismic anisotropy

CPO data, also referred to as texture or crystallographic fabric, were obtained using indexation of EBSD patterns (EBSP) generated on a JEOL5600 scanning electron microscope (SEM-EBSD, Geosciences-Montpellier, France). This EBSP-indexation is obtained from the comparison between acquired and simulated diffraction patterns for each analysis point using HKL CHANNEL 5+ software (Schmidt and Olesen, 1989). Mean angular deviation (MAD), which shows the match of the overlap of the measured diffraction pattern by the simulated EBSB, was commonly <1° (mainly ~0.6°). Euler angles (φ1, ϕ, and φ2) characterizing 3D orientation of crystal lattice were

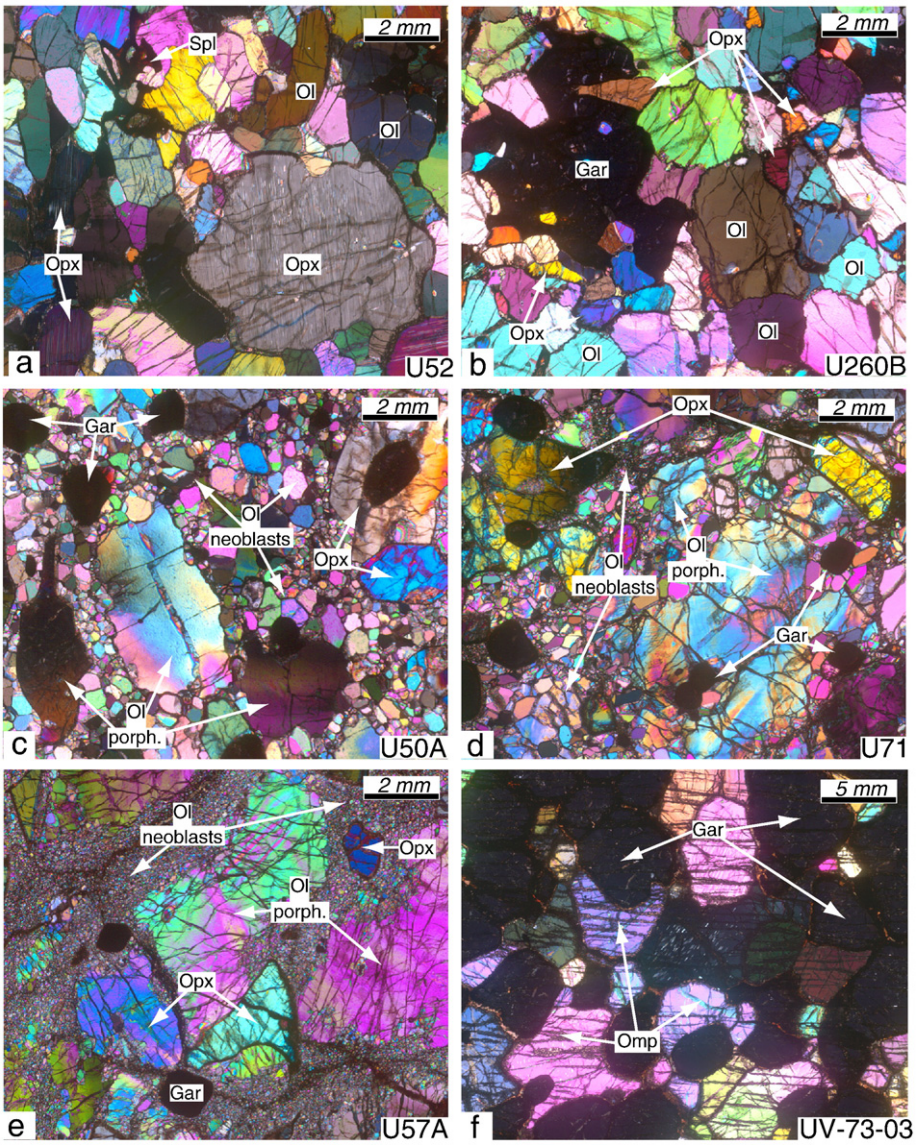

Fig. 2. Photomicrographs (crossed polarizers) showing typical microstructures of the Udachnaya xenolith suite: (a) coarse spinel peridotite, (b) coarse garnet peridotite, (c–e) porphyroclastic garnet peridotites and (f) eclogite; sample numbers are shown at bottom right. Porphyroclasts of garnet peridotites display typical substructure, which suggests dislocation-flow. Porphyroclastic peridotite U57A (e) shows a well-developed mosaic, fine-grained matrix.

measured in automatic mode with sampling steps ranging from 50 to 100 μm depending on mean grain size. Measurements of olivine porphyroclasts for sample 70A that were carried out grain-by-grain using operator-controlled indexing procedure have been added to the CPO data. Indexation rates for automatic mode measurements are generally better than 80% (~95% for 3 samples). To increase precision, only measurements with MAD <1° are taken into account.

The CPO of minerals is displayed as pole figure, equal area and lower hemisphere in Figs. 5–7 based on all available measurements, except for olivine porphyroclasts in sample U57A and for clinopyroxene and garnet in eclogites, for which the data were recalculated and represented using average Euler angles for each grain. The latter plotting method avoids over-representation of larger grains (notably garnet). When visible in the xenoliths, lineation and foliation were also shown in respective projections. The fabric strength of olivine for peridotites and of cpx for eclogites is indicated for each projection as dimensionless J texture-index (Bunge, 1982); it equals unity for a random distribution and tends to infinity for a single crystal.

3.1. Olivine CPO

In coarse peridotites, foliation and lineation are difficult to define and are not reported in Fig. 5a,b, except for U15 and U52. In these two samples, the maximum concentration of [100] is parallel to lineation, [010] is perpendicular or tends to form a girdle perpendicular to the foliation (U15 and U52, respectively), and [001] is in the foliation plane perpendicular to the lineation. Coarse peridotites mainly have orthorhombic CPO with stronger clustering (highest MD values) for [100]. In addition, spinel peridotites also show fiber-[100] CPO type (Bunge, 1982) characterized by strong concentration of [100] and by distribution in girdle of [010] and [001], e.g. for U504 and U52. Coarse garnet peridotites yield fabric strengths around 4.5 (J_{index} from 4.08 to 5.74). J_{index} values in spinel peridotites have a broader range from 3.56 (U225A) to 11.00 (U15).

Porphyroclastic peridotites mainly have orthorhombic type CPO with well-defined clustering of [100], [010] and [001] (Fig. 5c). The maximum of density (MD number) also indicates that the concentration of crystallographic axes is commonly the highest for [010]. The CPO

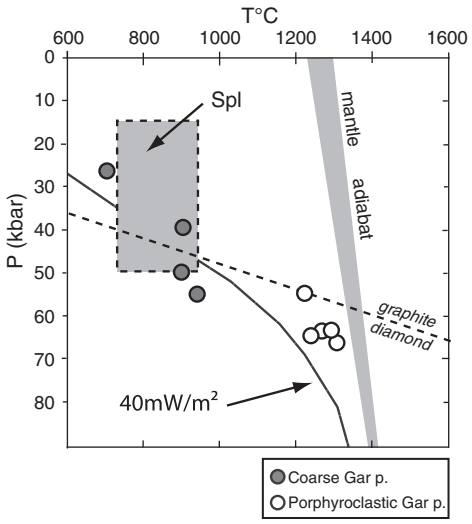

Fig. 3. A plot of equilibration temperatures versus equilibration pressures for xenoliths in this study (black circles, coarse spinel peridotites; gray circles, coarse garnet peridotites; and empty circles, porphyroclastic peridotites). Temperatures are from the cpx–opx thermometer of Taylor (1998) for garnet peridotites and the Ca-opx method of Brey and Kohler (1990) for spinel peridotites. Pressures are from the opx-gar barometer of Nickel and Green (1985). Gray rectangle delimits the field of likely P-T conditions for spinel peridotites (a pressure of 25 kbar was assumed to calculate T values for spinel peridotites). Shown for reference are: conductive model geotherm of Pollack and Chapman (1977) corresponding to a surface heat flow of 40 mW/m^2, mantle adiabat and the graphite–diamond transition boundary (Rudnick and Nyblade, 1999).

appears to be related to foliation and lineation in porphyroclastic rocks. The strongly concentrated [010] is close to the foliation pole, except for the near random fabric of U267 ($J_{index}=2.22$) for which [010] is located at 45° of the foliation pole. The concentration maximum of [100] lies in the foliation plane and tends to be close to the lineation (U71, U50A, and U70A). Except for U183A, [001] orientation is slightly weaker in comparison to [100] and [010]. The concentration maximum of [001] is commonly located in the foliation, at high angle of the lineation for U71. We note a weak concentration maximum of [001] close to the lineation for U50A. For U9D and U70A, the high concentration of [001] forms relatively individualized sub-maxima in the foliation plane. The fabric

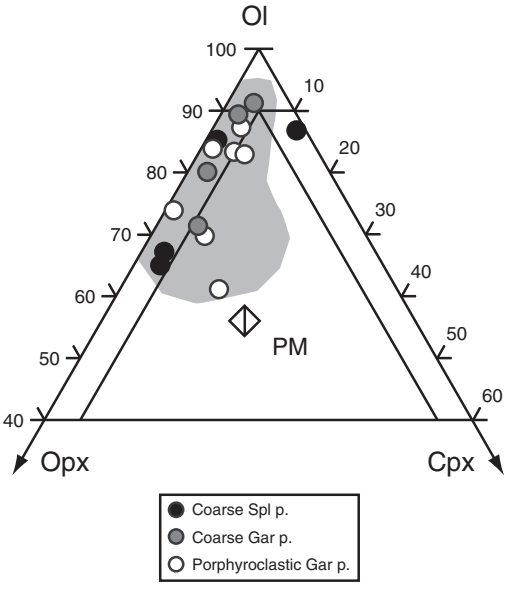

Fig. 4. Triangular modal composition diagram for peridotites in this study (data from Table 1); symbols are same as in Fig. 3; PM, primitive mantle estimate. Gray field outlines modal compositions of a larger suite of Udachnaya peridotites after Ionov et al. (2010).

strength of porphyroclastic peridotites ranges from 2.22 to 8.07. Samples characterized by mosaic microstructures in the matrix systematically display low J_{index} values (<3.5). Fig. 5c shows olivine CPO for both porphyroclasts and the fine-grained matrix of sample U57A. The recrystallized grains appear to have a more diffuse preferred orientation than the porphyroclasts. This results in lower fabric strength for the neoblasts ($J_{index}=2.67$) than for the porphyroclasts ($J_{index}=5.80$) with similar pattern (i.e., the highest density maximum for [010]). In addition the [100] and [010] concentration maxima of neoblasts are very close to those of porphyroclasts. The [001] of neoblasts is almost randomly oriented.

3.2. Pyroxene and garnet CPO

Fabric patterns are more diverse for opx than for olivine. However, in porphyroclastic and in spinel peridotites, in which the foliation and lineation are visible, the opx fabrics mainly show alignment of [100] perpendicular to foliation, [010] close to foliation and normal to lineation, and [001] parallel to lineation (e.g. in U52 and U71, Fig. 6). A subsidiary fabric pattern shows an alignment of [001] close to lineation, [010] perpendicular to foliation and [100] normal to lineation in foliation (U50A, Fig. 6).

CPO of cpx in peridotites is characterized by alignment of [001] close to lineation. The distribution of (100) and (010)-poles is generally more complex for cpx than for opx. For example, (010)-pole forms: (i) one maximum perpendicular to the lineation in the foliation plane in U52, (ii) maxima close to the foliation pole and to the lineation in U71 and (iii) two maxima at high angle from the foliation pole in U50A (Fig. 6). CPO of cpx in eclogites (Fig. 7a) shows a clear alignment of [001] close to lineation; the (010)-poles tend to form a girdle perpendicular to lineation with a concentration maximum close to the foliation pole for sample UV-KC-147. The fabric strength of cpx in eclogites is very high, with J_{index} above 10.

Garnets in peridotites show neither shape-preferred orientation nor preferred alignment of crystallographic axes. Garnet grains in eclogites mainly have round shapes, and their CPO patterns appear to be almost randomly oriented (Fig. 7b).

3.3. Seismic properties

3D seismic properties of the xenoliths were modeled using single-crystal elastic constants, density, CPO and modal proportions of minerals with the method of Mainprice and Humbert (1994). Proportions of major minerals (olivine, opx, cpx and garnet or spinel for peridotites, and cpx and garnet for eclogites) used in the calculations are from Table 1. Seismic properties are computed using the software of Mainprice (1990), with Voigt–Reuss–Hill averaging of single-crystal elastic constants (Abramson et al., 1997; Babuska et al., 1978; Chai et al., 1997, Collins and Brown, 1998; Duffy and Vaughan, 1988; Li et al., 1995). The elastic stiffness matrix and the density of olivine were calculated taking into account $Mg\#_{ol}$. In addition, we have considered a pyrope composition for peridotitic garnets, and a pyrope (40%), almandine (40%), grossular (20%) composition for eclogitic garnets.

Calculated seismic properties are summarized in Table 1 and shown in Fig. 8 for peridotites and eclogites. The 3D-results are displayed in lower hemisphere and structural reference frame (X, Y, and Z) projections with foliation and lineation for representative samples.

P-wave velocity patterns of all peridotites are quite similar. The fastest P-wave propagation (Vp_{max}) is in the direction of the X structural axis (lineation). The low velocities are normal to the structural XY-plane (foliation), with minimum of velocity (Vp_{min}) usually close to Z axis. For coarse garnet peridotites, the Vp_{max} ranges from 8.48 to 8.85 km/s and the Vp_{min} from 8.09 to 8.20 km/s, with a Vp anisotropy range of 4.4–9.0%. The most extreme Vp and AVp values

are obtained for spinel peridotites, with Vp_{max} of 8.58–9.02 km/s, Vp_{min} of 7.97–8.18 km/s and AVp of 5.5–11.5%. For porphyroclastic rocks, the Vp_{max} ranges from 8.36 to 8.64 km/s and the Vp_{min} from 8.03 to 8.19 km/s, resulting in a Vp anisotropy (AVp) range of 2.8–7.5%. The lowest AVp values are for rocks most affected by recrystallization (U267 and U183A), whereas the least recrystallized xenolith U71 yields the highest anisotropy (AVp = 7.50%).

S-wave velocity patterns of peridotites show more sample-to-sample variation than P-wave patterns. For spinel peridotites, the highest Vs anisotropy values (AVs) tend to form a girdle normal to lineation, with the lowest values close to lineation. For porphyroclastic rocks, the highest AVs lie in the foliation plane and the lowest define a high angle with the Y and X axes. The highest AVs_{max} value (8.01%) is obtained for spinel peridotite U504; the lowest (2%) is for xenolith U183A, which is the one most affected by recrystallization. The range of sample-to-sample Vs variation is limited, with average $Vs1_{max}$ of 5.00 km/s for spinel, 4.97 km/s for coarse garnet and 4.95 km/s for porphyroclastic peridotites. The fast S-wave tends to be polarized in a plane containing its propagation direction and the lineation.

Seismic patterns for eclogites (Fig. 8b) are more complex than for peridotites with respect to foliation and lineation. The P-wave velocity maximum is high (average Vp_{max} 8.73 km/s). On the other hand, seismic anisotropy is very weak (AVp ≤2.5%; AVs_{max} <2%). Calculated seismic velocities and anisotropies are in agreement with those observed in fresh eclogites from various localities (e.g., Bascou et al., 2001; Mauler et al., 2000; Wang et al., 2005).

The pyroxenite (Table 1) has low P- and S-wave velocities (Vp <8 km/s; Vs <5 km/s) and anisotropy (AVp 2.2%, AVs_{max} 2.07%) compared to peridotites and eclogites.

4. Discussion

4.1. Microstructures, crystallographic fabrics and deformation

CPO developed under lithospheric conditions is well preserved in the Udachnaya xenoliths, despite evidence for grain-boundary mobility in coarse peridotites, such as lobate grain boundaries and low densities of intra-crystalline deformation features. Microstructures and CPO patterns indicate that the deformation essentially took place in the dislocation creep regime. Olivine CPO patterns for peridotites with observable foliation and lineation suggest a dominant activation of the (010) [100] slip system as is common for natural deformed peridotites (e.g., Nicolas and Poirier, 1976).

The general CPO pattern of olivine in the coarse and porphyroclastic samples is very similar, but there are some differences. Coarse peridotites show a better alignment of [100]-olivine while porphyroclastic rocks have a better alignment of [010]-olivine. The causes of differences in clustering of crystallographic axes in CPO patterns remain poorly understood. Numerical models of olivine CPO development (assuming that deformation is accommodated by dislocation glide; Tommasi et al., 1999) produce, in simple-shear regime, orthorhombic patterns characterized by stronger [100] clustering and weaker [010] clustering. The development of patterns with better clustering of [010] observed in porphyroclastic rocks from Udachnaya is less straightforward. This could be due to increased activity of the secondary (010) [001] slip system as suggested by CPO displayed by porphyroclastic samples (U50A and U70A). In addition, the development of bimodal CPO pattern with two maxima of [100] and [001] close to the foliation plane (which characterizes sample U9D) could be facilitated through the increase of the (010) [001] slip system during deformation.

The presence of water and melt may change the dominant slip direction of olivine from [100] to [001] (Jung and Karato, 2001). This could explain olivine CPO indicating [001] slip as observed in naturally deformed peridotites from the mantle wedge above a subducting slab in southwest Japan (Michibayashi et al., 2007; Tasaka et al., 2008). Strain partitioning due to the presence of oriented melt pockets may also develop significant concentration of [001] axes parallel to the shear direction (Holtzman et al., 2003). However, melt-rich pockets or bands are not observed in Udachnaya xenoliths, even though these samples are affected by metasomatism, in particular porphyroclastic samples that show the highest enrichments in TiO_2, rare earth elements (REE) and other incompatible trace elements (Ionov et al., 2010).

Numerical models of olivine CPO development (Tommasi et al., 1999) show that [010] strengthening and development of girdle distribution in the foliation plane for [100] and [001] could also be formed in response to axial shortening. In this hypothesis, it is expected that the development of CPO patterns for opx is affected in the same manner considering the activation of dominant opx slip system, i.e. the strengthening of (100). However, in porphyroclastic samples, the dominant slip plane (100) is not systematically more concentrated than (010) and (001) suggesting that the observed difference between the olivine CPO patterns is not related to deformation regime.

Olivine CPO patterns suggesting significant contribution of [001] slip were also observed for mantle xenoliths in the Kapvaal (Boullier and Nicolas, 1975) and the Tanzanian cratons (Vauchez et al., 2005). Experimental results (Couvy et al., 2004; Mainprice et al., 2005) have shown that the dislocation slip in the [001] direction is related to conditions of high-pressure (and high-temperature) deformation. The (010) [001] slip system could be then be easily activated near the base of the cratonic mantle (>180 km). Thus, a larger activation of [001] slip simultaneous with the dominant activation of [100] slip direction during deformation under high pressure may be favored to explain the strengthening of [010] in olivine CPO patterns of porphyroclastic peridotites from Udachnaya.

Microstructures with large deformed porphyroclasts set in a fine-grained matrix are rare in peridotites equilibrated at high T's (>1100 °C) and are more common in peridotites from medium- to low-T domains in shear zones (e.g., Michibayashi et al., 2006; Vissers et al., 1995). The deformation mechanisms in these 'tectonites' involve dislocation creep with associated dynamic recrystallization that results in grain size reduction and the development of a fine-grained matrix (e.g., Nicolas and Poirier, 1976). High-T, deformed peridotite xenoliths from kimberlites appear to be a particular case resulting from very high-stress and high strain-rate deformation (e.g., Goetze, 1975; Mercier, 1979). For these rocks, the development of recrystallization microstructures could take place in two stages: large numbers of fine-grained neoblasts form initially by dynamic recrystallization, and a subsequently selective growth of some of them (Drury and Van Roermund, 1989). These authors argue that the growth process could produce euhedral "tablet-shaped" grains during static recrystallization by fluid-assisted grain boundary migration.

The recrystallized grains appear to have a more diffuse preferred orientation than the porphyroclasts (see olivine CPO of porphyroclasts and neoblasts for U57A). This randomization of a pre-existing CPO in the finest-grained region in a given rock could correspond to a change in deformation; the latter may be due to grain boundary sliding as suggested by Boullier and Gueguen (1975).

Deformation in eclogites mainly takes place in cpx. CPO patterns of cpx in eclogites are quite similar suggesting a dominant activation of (010) [001] during deformation. However, no significant activity of this slip system has ever been observed in naturally and experimentally deformed eclogites (Buatier et al., 1991; Godard and Van Roermund, 1995). A recent study on a single diopside crystal deformed at high P-T conditions confirms the non-contribution of slip on (010) and the dominant activation of slip on {110} (Amiguet et al., 2010). Numerical simulations of CPO development for cpx (Bascou et al., 2002) have showed that the dominant activation of {110} slip planes could generate CPO with [010] normal to foliation, in spite of the lack of (010) [001] slip system activation.

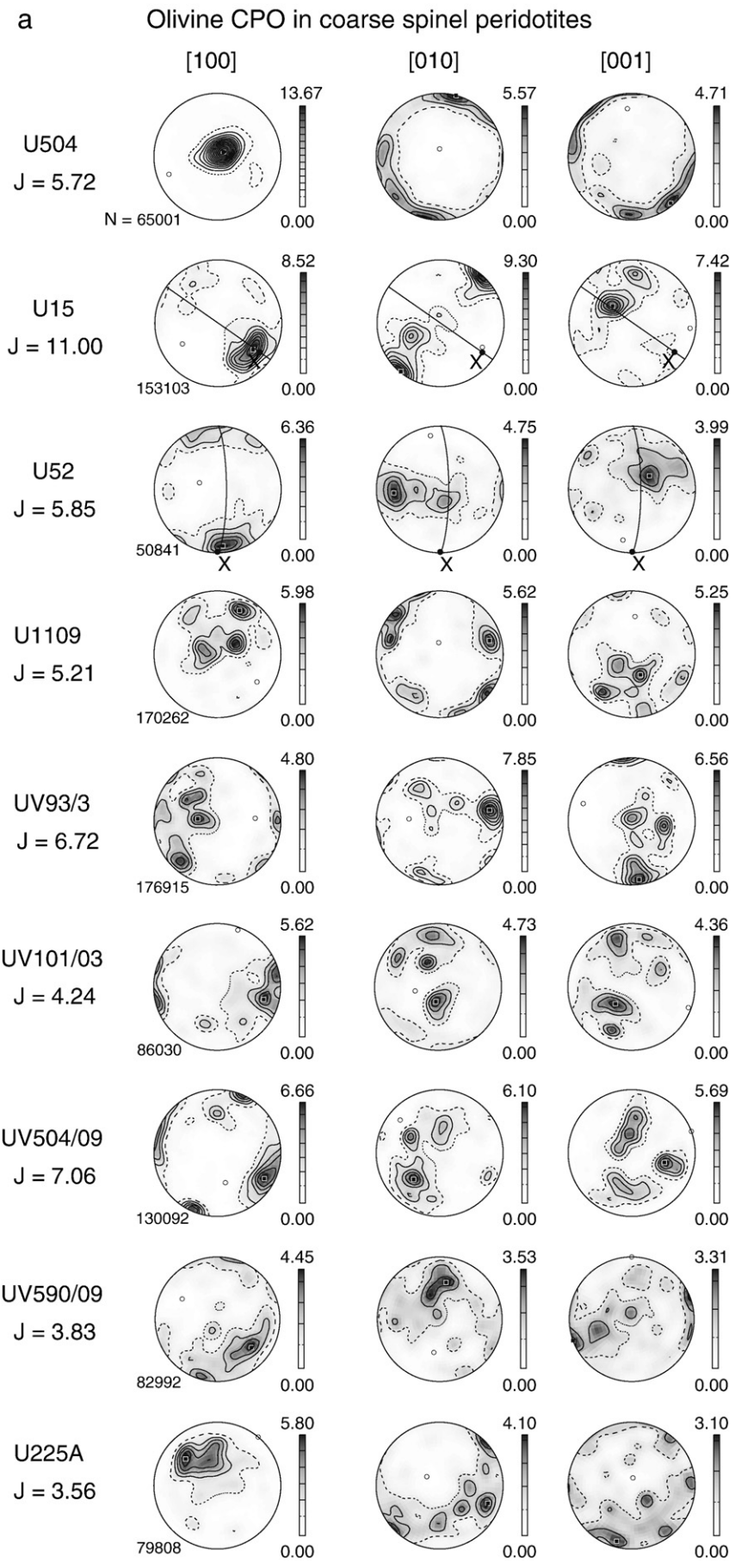
a
Olivine CPO in coarse spinel peridotites
[100]
[010]
[001]
U504
J = 5.72
N = 65001
13.67
5.57
4.71
0.00
U15
J = 11.00
153103
8.52
9.30
7.42
U52
J = 5.85
50841
6.36
4.75
3.99
U1109
J = 5.21
170262
5.98
5.62
5.25
UV93/3
J = 6.72
176915
4.80
7.85
6.56
UV101/03
J = 4.24
86030
5.62
4.73
4.36
UV504/09
J = 7.06
130092
6.66
6.10
5.69
UV590/09
J = 3.83
82992
4.45
3.53
3.31
U225A
J = 3.56
79808
5.80
4.10
3.10

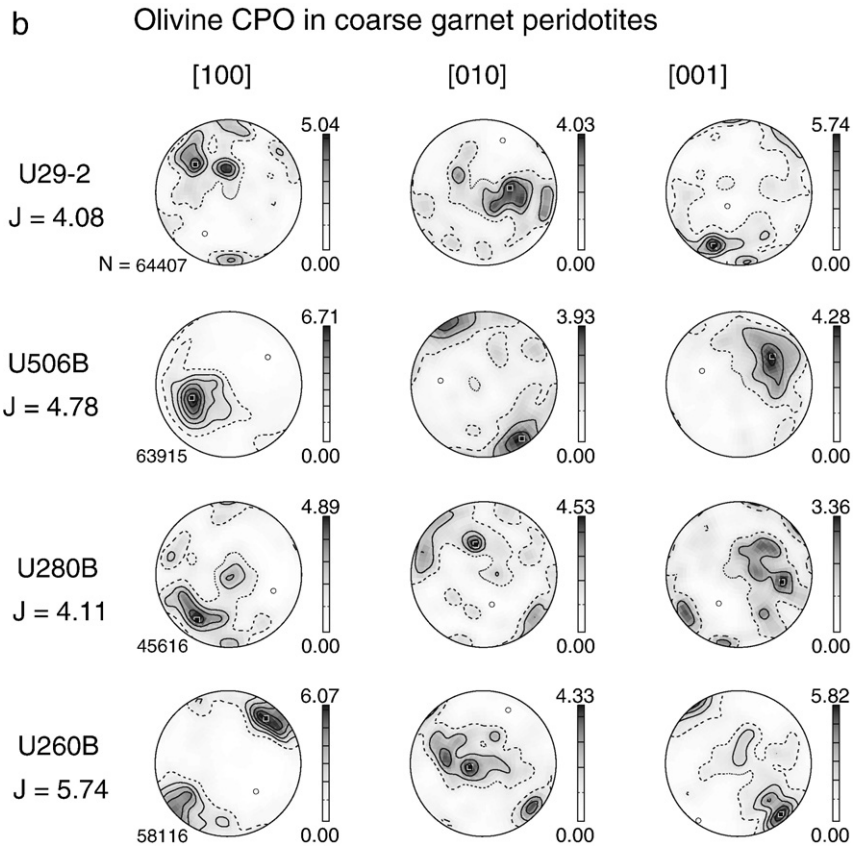

Fig. 5. Olivine CPO patterns of peridotites: (a) coarse spinel samples, (b) coarse garnet samples, and (c) porphyroclastic garnet samples. CPO are represented on equal area, lower hemisphere projection from individual measurements except for olivine porphyroclasts from sample U57A that are represented using average Euler angles for each grain. Foliation, when observed, is marked by a black line. Lineation, when determined, is marked by the structural axis X. The density contours are in Multiple Uniform Distribution (MUD); N is the number of measurements. The olivine fabric strength is given by the J_{index} number.

4.2. Crystallographic fabrics and seismic velocities

Olivine is highly anisotropic, with the fastest P-wave velocity (and shear-wave polarization) parallel to the [100] axis. The intermediate and minimum P-velocities are respectively parallel to the [001] and [010] axes (Birch, 1961). Olivine fabrics database of Ben Ismaïl and Mainprice (1998) describes relationships between seismic properties of peridotites and olivine CPO. The P-wave anisotropy is largely controlled by olivine [100] alignment whereas the S-wave anisotropy is sensitive to contributions from all three axes ([100], [010] and [001]). Moreover, Ben Ismaïl and Mainprice (1998) show that seismic anisotropy increases with olivine fabric strength for both P- and S-waves.

For the Udachnaya suite, coarse peridotites show the greatest P-wave velocity anisotropy (>8%) and the fastest P-wave velocities (Vp max>8.7 km/s) (Fig. 9a,b). These samples have weak to moderate fabric strength (J_{index} from 3.3 for U225A to 7 for UV504/09) and relatively high olivine contents (80 to 90%). The olivine CPO symmetry is marked by a higher concentration of [100] with regard to [010] and [001] (e.g., U504, U260B, and U225A, Fig. 5). By contrast, coarse peridotite U15, which has a distinctive olivine CPO pattern symmetry (best alignment for [010]), displays the highest fabric strength ($J_{index}=11$), low olivine content (65%), moderate P wave anisotropy (AVp=7.6%) and Vp velocity ($Vp_{max}=8.6$ km/s). These results underline the effects of olivine content and olivine CPO symmetry patterns (strong alignment of olivine [100] for coarse peridotites) on seismic P-wave anisotropy that favor very high Vp values for peridotites. The effect of recrystallization that affects the fabric strength of olivine (see J_{index} values for porphyroclasts and neoblasts from sample U57A in Fig. 5c) on P-wave anisotropy is also apparent in sample U267 that shows both the lowest J_{index} (=2.22) and the lowest AVp (2.80%). The restricted correlation between the P-wave anisotropy and the fabric strength of olivine underlines the effects (volume and CPO) of other minerals in particular of opx and cpx. Variations of seismic velocities are smaller for S-waves than for P-waves (Table 1).

In eclogites, the effect of major deformed mineral fabric (cpx) on seismic properties differs from the effect of olivine fabric for peridotites. Because the density of eclogites is higher than for peridotites, the seismic velocity averages (Vp_{ave} and Vs_{ave}) are the highest for eclogites ($Vp_{ave}=8.65$ km/s, $Vs_{ave}=4.94$ km/s in eclogites; $Vp_{ave}=8.40$ km/s, $Vs_{ave}=4.86$ km/s in coarse spinel peridotites). On the other hand, because anisotropy is little developed in the eclogites (AVp and AVs <3%), their seismic velocities are little affected when the anisotropy is taken into account (Fig. 9d). As a result, the P-wave velocities calculated for some peridotites exceed those for the eclogites (Vp ≥8.8 km/s) due to the high anisotropy of the peridotites.

4.3. P-wave anisotropy calculations versus seismic records for the lithospheric mantle in the Siberian craton

The modeled 3D seismic properties in this study are characterized by large P-wave anisotropy, in particular for coarse peridotites. Seismic velocities calculated from our CPO data and modal abundances of major phases are higher than the measured velocities in two porphyroclastic and one coarse peridotites from Udachnaya by Kobussen et al. (2006). The latter paper also reports calculated seismic properties for their three peridotite xenoliths assuming that they only contain olivine (i.e. disregarding other minerals). Their estimates for the porphyroclastic

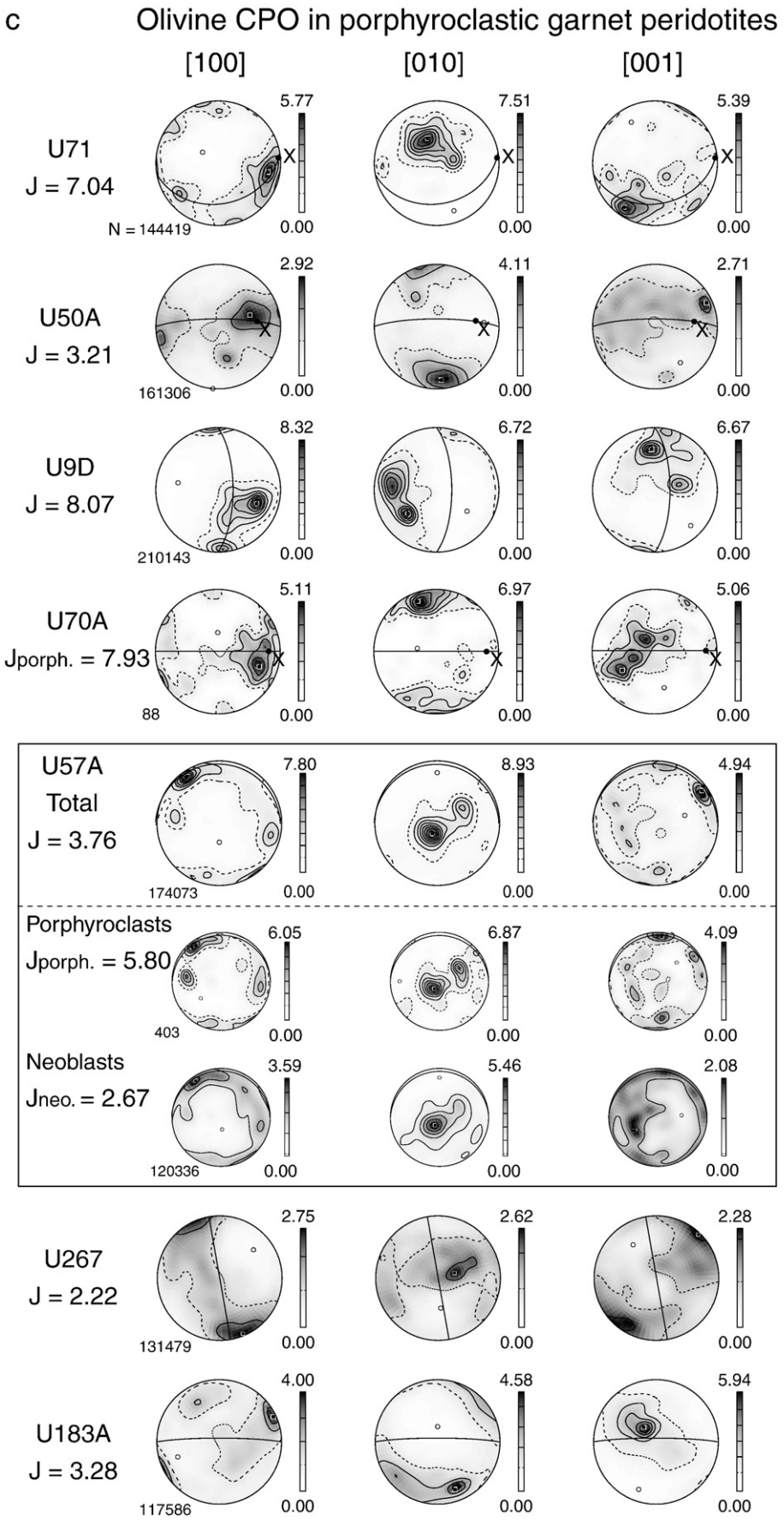

Fig. 5 (*continued*).

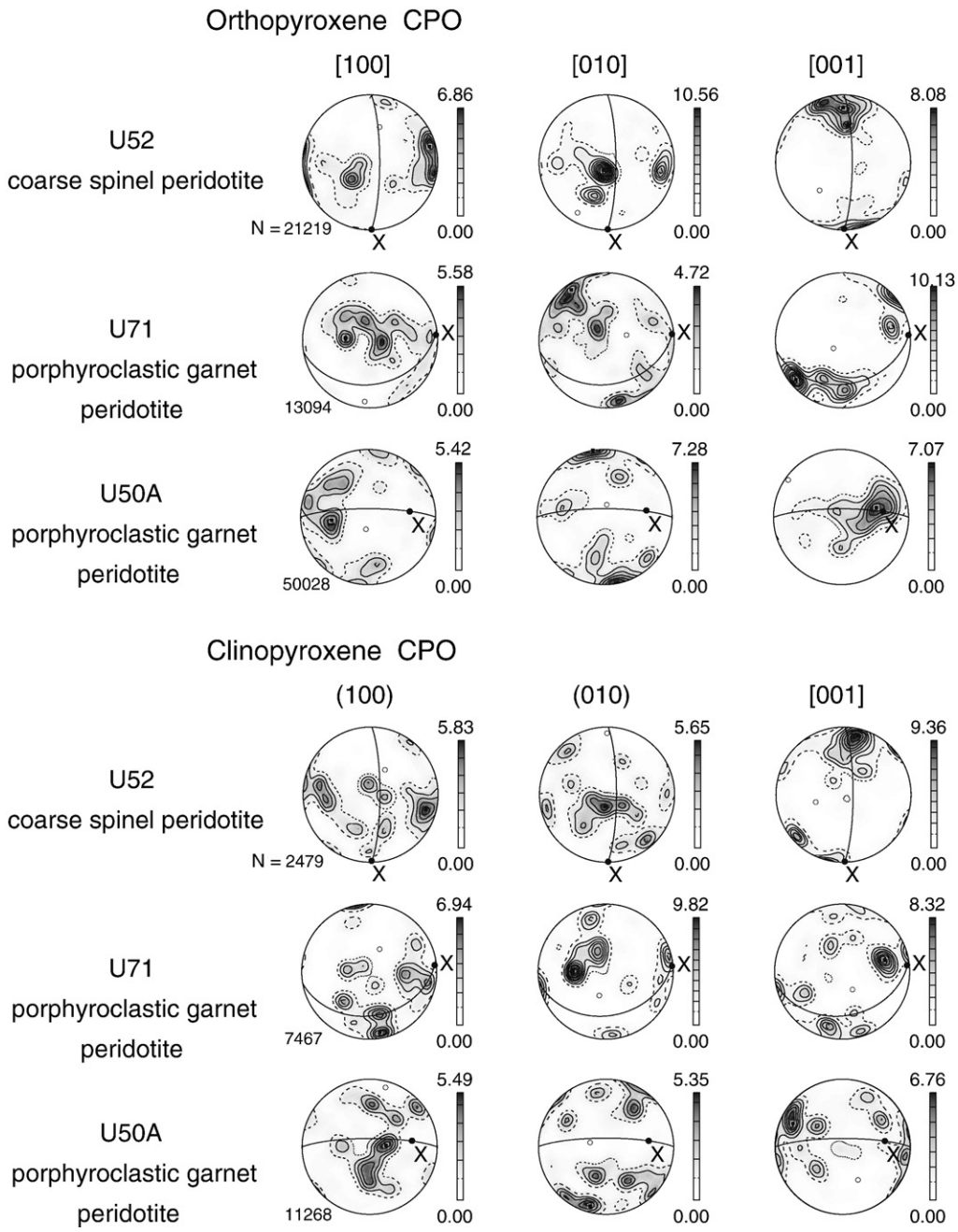

Fig. 6. Representative orthopyroxene and clinopyroxene CPO of Udachnaya peridotites, for which foliation (black line) and lineation (X-axis) are observed. CPO are presented on equal area, lower hemisphere projection from individual measurements. The density contours are in Multiple Uniform Distribution (MUD); N is the number of measurements.

rocks yield higher-velocity patterns due to oversimplification of modal mineralogy, but probably also to under-evaluation of the effects of matrix recrystallization.

Differences in P-wave velocities along two perpendicular seismic profiles in Siberia have been identified by Suvorov et al. (2006). Vertical variations have been also mapped from four Peaceful Nuclear Explosion events along the East–West "Craton" seismic profile (Nielsen et al., 1999, 2002). The latter authors provide evidence for a zone with slightly reduced P-wave velocity in the 100–200 km depth range. In addition, a combined analysis of SKS splitting and P travel times in three long-range profiles suggests the existence of lateral and vertical zones with different velocities beneath the "Craton" profile including a low velocity zone between 150 and 250 km (Oreshin et al., 2002). The rock anisotropy could explain the recorded high-Vp velocities (>8.5 km/s) and the horizontal and vertical variations mapped in the upper mantle of central Siberian craton. However, as emphasized by Suvorov et al. (2006), anisotropy as a cause of seismic observations is not unequivocal. Abrupt compositional changes due to local concentration of unusual rocks such as garnet-rich eclogites or pyroxenites, could produce abrupt velocity variations in the sub-Moho mantle as suggested by the distinct seismic properties estimated for peridotites, eclogites and pyroxenite in this study. Domains of 'frozen' anisotropic zones of variable orientations, originating from localized deformation associated to the amalgamation of terrains resulting in the formation of the Siberian craton, could be equally invoked to explain the observed sharp seismic variations in the seismic profiles.

Petrologic and geochemical studies (e.g., Boyd et al., 1997; Griffin et al., 1999; Ionov et al., 2010) suggest that the lithospheric mantle beneath central Siberian craton was variably affected by metasomatism. The porphyroclastic peridotites are believed to have experienced the

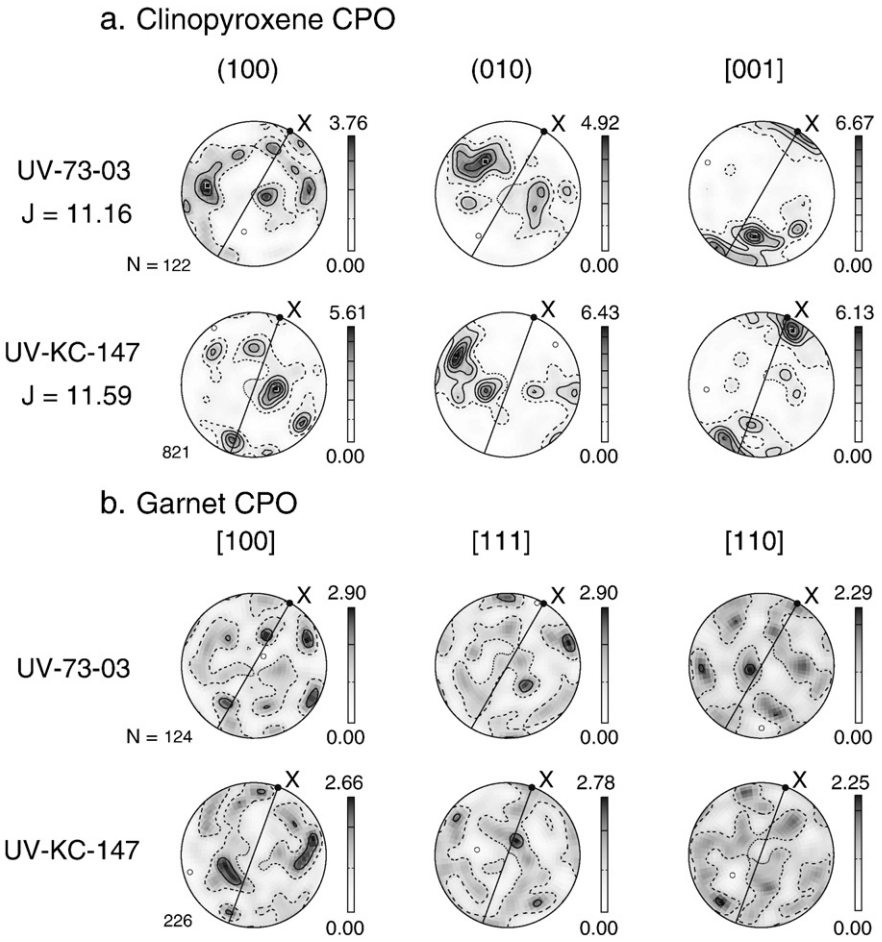

Fig. 7. CPO patterns for clinopyroxene (a) and for garnet (b) in eclogites. CPO are presented on equal area, lower hemisphere projection using average Euler angles for each grain in order to avoid the over-representation of larger grains (notably garnet). Foliation is marked by a black line and lineation by the structural axis X. The density contours are in Multiple Uniform Distribution (MUD); N is the number of measurements.

strongest metasomatism and delineate a zone of intense melt-rock interaction at the base of the lithosphere. The estimate of ~210–220 km for the lithosphere–asthenosphere transition is in line with seismic observations using Deep Seismic Sounding techniques of Egorkin et al. (1987b), which indicate a clear decrease in Vp (up to 0.4 km/s) commonly viewed as the Lehman Discontinuity. It is also consistent with regional tomography from P-, S- and Rayleigh-waves (Kulakov, 2008; Priestley et al., 2006).

Microstructures in the Udachnaya porphyroclastic peridotites indicate that the base of the lithospheric mantle has been intensely deformed. The high fabric strength measured from porphyroclasts of olivine ($J_{porph}>5$) suggests a strong seismic anisotropy. However, the seismic anisotropy and the velocities calculated for these xenoliths are not particularly high (average of Vp_{max} around 8.5 km/s) due to recrystallization and the development of fine-grained matrix that reduces the fabric strength. Specific types of fabric patterns (preferential alignment of [010]) of olivine may also play a role. By contrast, coarse spinel peridotites, which are dominant in the sub-Moho mantle, yield very high-calculated P-velocities in agreement with seismic data from the Siberian craton.

5. Conclusions

Seismic properties of typical cratonic mantle rock types have been estimated from CPO data and modal compositions for a representative suite of xenoliths from the Udachnaya kimberlite. Microstructural observations, crystallographic fabric measurements and calculations of seismic properties suggest the following:

1. The CPO of olivine is characterized by a stronger alignment of [100] in coarse peridotites and of [010] in porphyroclastic peridotites. The olivine fabric strength is the highest in coarse spinel harzburgites. In porphyroclastic peridotites, recrystallization leads to the reduction in olivine grain size and the development of a mosaic, randomly oriented matrix, and thus decreases the fabric strength. In samples with apparent foliation and lineation, the CPO of olivine shows a concentration of [100] close to the lineation and of [010] perpendicular to the foliation.
2. The dominant deformation mechanism appears to be dislocation creep a microstructures and the CPO of olivine and pyroxenes in peridotites and of cpx in eclogites. The dominant slip systems in peridotites are (010) [100] for olivine and (100) [001] for opx. The less common slip systems (010) [001] for olivine and for opx could also be activated in some porphyroclastic rocks. Clinopyroxene shows a clear slip direction on [001] both in peridotites and eclogites.
3. Seismic properties of porphyroclastic and coarse peridotites show some differences. Maximum P-wave velocities are higher in the coarse rocks, with the highest velocity ($Vp_{max}=9$ km/s) found for a spinel harzburgite. For S-waves, CPO pattern variations mainly affect the spatial distribution of anisotropy. The maximum of anisotropy is in the foliation plane. The minimum of anisotropy is oriented at a high angle to the foliation plane for porphyroclastic

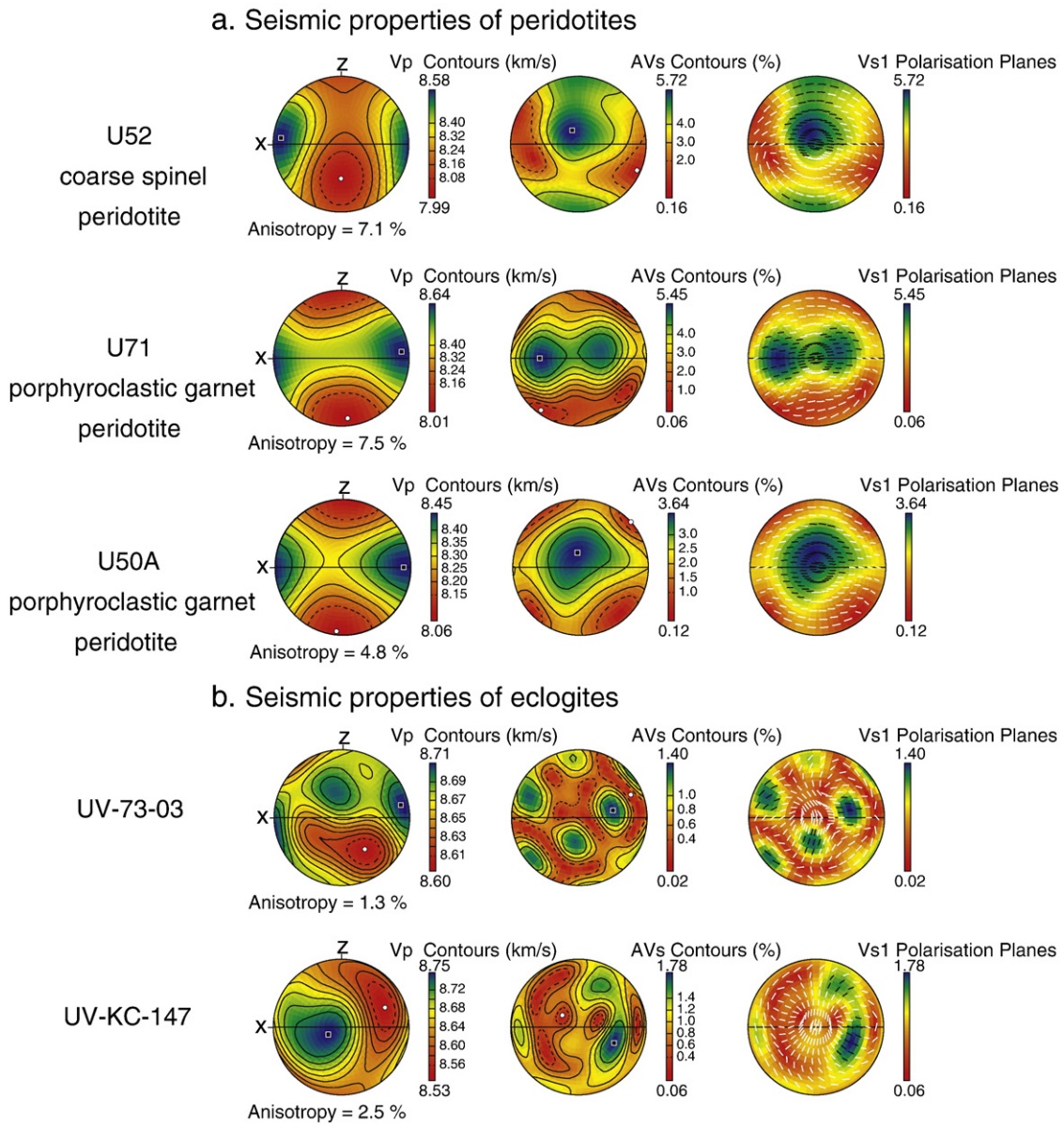

Fig. 8. Representative patterns of seismic properties of Udachnaya xenoliths, for which foliation and lineation are observed. Equal area, lower hemisphere projection in the structural reference frame X, Y, and Z. Full line: foliation (XY plane) is vertical and lineation (X) is horizontal. This figure presents P-wave velocity (Vp km/s), the anisotropy of P-waves (AVp%) defined as $100\times[(Vp_{max}-Vp_{min})/(Vp_{max}+Vp_{min})/2]$, the anisotropy of S-waves (AVs%) defined for a specific direction as $100\times[(Vs_1-Vs_2)]/[(Vs_1+V_2)/2]$ where Vs_1 and Vs_2 are respectively the fast and slow S-wave velocities and the direction of the Vs_1 polarization planes.

peridotites but parallel to the lineation for coarse peridotites. The phase transition between spinel and garnet peridotites does not involve important changes in Vp and Vs velocities and thus may be difficult to detect using seismic methods.

4. In isotropic models, the eclogites have distinctively higher P-wave velocities (~8.65 km/s) than peridotites and pyroxenites because of high modal garnet, hence high rock density. In a more realistic anisotropic model, however, some coarse peridotites yield much higher P-wave velocities in the fast direction, which overlap those for the eclogites. Such peridotites, particularly spinel harzburgites, appear to be the best candidates to explain the extremely large P-wave velocities in the sub-Moho mantle in the vicinity of kimberlite fields in central Siberia.

Acknowledgments

We thank N. Pokhilenko for support of this project, C. Alboussiere for preparation of high-quality polished sections for EBSD measurements, A. Tommasi for facilitating access to SEM-EBSD instrument at Montpellier University, F. Barou for technical assistance and D. Mainprice for providing software to generate pole figures and calculate seismic properties. We also thank M Michibayashi and A. Vauchez for their helpful reviews. D. Ionov acknowledges financial support in 2010 from the French CNRS (PNP-INSU grant) and the University of Saint Etienne (Actions Internationales de la Recherche); A. Golovin acknowledges RFFI grant no. 10-05-00575-a.

Appendix A. Supplementary data

Supplementary data to this article can be found online at doi:10.1016/j.epsl.2011.01.016.

References

Abramson, E.H., Brown, M., Slutsky, L.J., Zaug, J., 1997. The elastic constants of San Carlos olivine up to 17 GPa. Journal of Geophysical Research 102, 12252–12263.

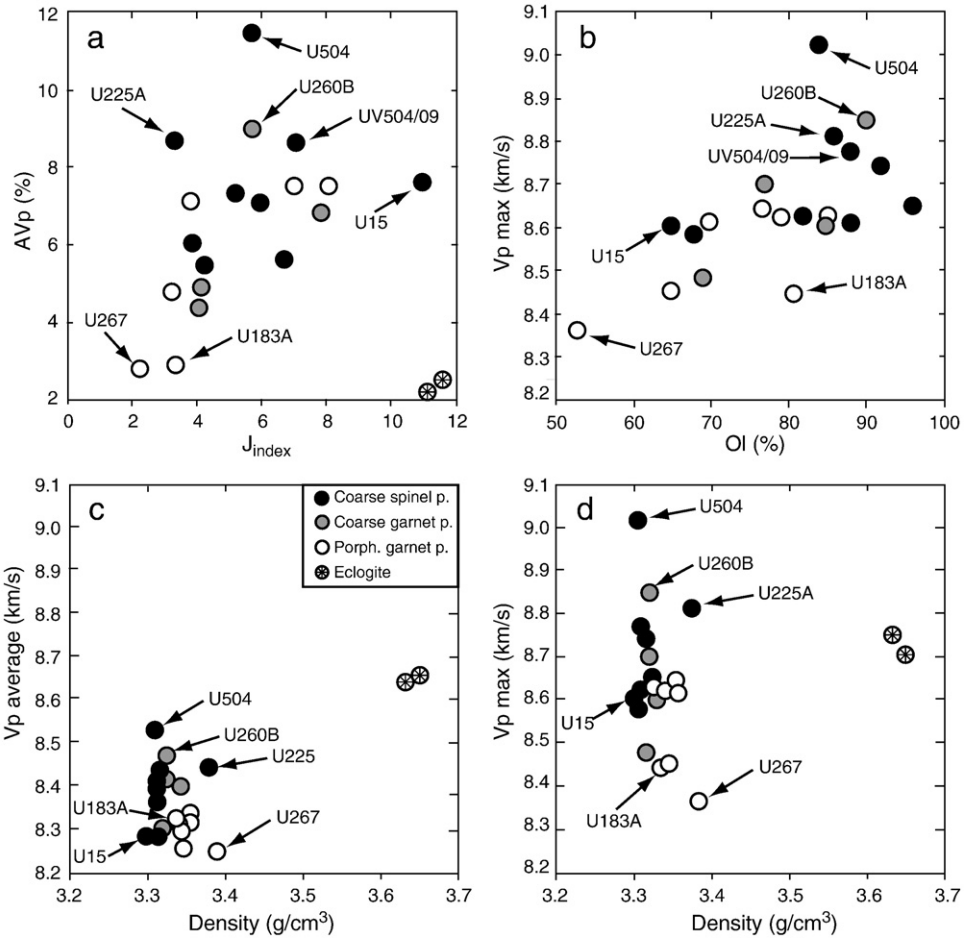

Fig. 9. P-wave velocity data for Udachnaya peridotites and eclogites: (a) a plot of AVp versus the fabric strength (J_{index}) of olivine for peridotites and of clinopyroxene for eclogites; (b) a plot of Vp_{max} versus modal olivine abundances (wt.%) for peridotites; (c and d) plots of Vp average and Vp_{max} versus calculated rock density (g/cm^3).

Amiguet, E., Cordier, P., Raterron, P., 2010. Deformation of diopside single crystals at mantle pressure. TEM characterization of dislocation microstructures. European Journal of Mineralogy 22, 181–187.

Artemieva, I.M., 2009. The continental lithosphere: reconciling thermal, seismic, and petrologic data. Lithos 109, 23–46.

Babuska, V., Fiala, J., Kumazawa, M., Ohno, I., 1978. Elastic properties of garnet solid–solution series. Physics of the Earth and Planetary Interiors 16, 157–176.

Bascou, J., Barruol, G., Vauchez, A., Mainprice, D., Egydio-Silva, M., 2001. EBSD-measured lattice preferred orientations and seismic properties of eclogites. Tectonophysics 342, 61–80.

Bascou, J., Tommasi, A., Mainprice, D., 2002. Plastic deformation and development of clinopyroxene lattice preferred orientations in eclogites. Journal of Structural Geology 24, 1357–1368.

Bascou, J., Delpech, G., Vauchez, A., Moine, B.N., Cottin, J.Y., Barruol, G., 2008. An integrated study of microstructural, geochemical and seismic properties of the lithospheric mantle above the Kerguelen plume (Indian Ocean). Geochemistry, Geophysics, Geosystems 9, Q04036, doi:10.1029/2007GC001879.

Ben Ismaïl, W., Mainprice, D., 1998. An olivine fabric database: an overview of upper mantle fabrics and seismic anisotropy. Tectonophysics 296, 145–157.

Birch, F., 1961. The velocity of compressional waves in rocks to 10 kbar, Part 2. Journal of Geophysical Research 66, 2199–2224.

Boullier, A.M., Gueguen, Y., 1975. SP-mylonites. Origin of some mylonites by superplastic flow. Contributions to Mineralogy and Petrology 50, 121–134.

Boullier, A.M., Nicolas, A., 1975. Classification of textures and fabrics of peridotites xenoliths from South African kimberlites. Physics and Chemistry of the Earth 9, 467–475.

Boyd, F.R., Pokhilenko, N.P., Pearson, D.G., Mertzmann, S.A., Sobolev, N.V., Finger, L.W., 1997. Composition of the Siberian cratonic mantle: evidence from Udachnaya peridotite xenoliths. Contributions to Mineralogy and Petrology 128, 228–246.

Brey, G.P., Kohler, T., 1990. Geothermobarometry in four-phase lherzolite; II, New thermobarometers, and practical assessment of existing thermobarometers. Journal of Petrology 31, 1353–1378.

Buatier, M., Van Roermund, H.L.M., Drury, M.R., Lardeaux, J.M., 1991. Deformation and recrystallization mechanisms in naturally deformed omphacites from the Sesia-Lanzo zone; geophysical consequences. Tectonophysics 195, 11–27.

Bunge, H.J., 1982. Texture Analysis in Materials Sciences. Butterworths, London.

Chai, M., Brown, J.M., Slutsky, L.J., 1997. The elastic constants of a pyrope-grossular-almandine garnet to 20 Gpa. Geophysical Research Letters 24, 523–526.

Collins, M.D., Brown, J.M., 1998. Elasticity of an upper mantle clinopyroxene. Physics and Chemistry of Minerals 26, 7–13.

Couvy, H., Frost, D.J., Heidelbach, F., Nyilas, K., Ungár, T., Mackwell, S., Cordier, P., 2004. Shear deformation experiments of forsterite at 11 GPa–1400 °C in the multianvil apparatus. European Journal of Mineralogy 16, 877–889.

Davis, G.L., Sobolev, N.V., Khar'kiv, A.D., 1980. New data on the age of Yakutian kimberlites obtained by the uranium–lead method on zircons. Doklady Akademii Nauk SSSR 254, 175–179.

Drury, M.R., Van Roermund, H.L.M., 1989. Fluid assisted recrystallisation in upper mantle peridotite xenoliths from kimberlites. Journal of Petrology 30, 133–152.

Duffy, T.S., Vaughan, M.T., 1988. Elasticity of enstatite and its relationships to crystal structure. Journal of Geophysical Research 93, 383–391.

Egorkin, A.V., Zuganov, S.K., Palenkova, N.A., Chernyshev, N.M., 1987a. Result of lithospheric studies from long-range profiles in Siberia. Tectonophysics 140, 29–47.

Egorkin, A.V., Zuganov, S.K., Pavlenkova, N.A., Chernyshev, N.M., 1987b. Results of lithospheric studies from long-range profiles in Siberia. Tectonophysics 140, 29–47.

Godard, G., Van Roermund, H.L.M., 1995. Deformation-induced clinopyroxene from eclogites. Journal of Structural Geology 17, 1425–1443.

Goetze, C., 1975. Sheared lherzolites; from the point of view of rock mechanics. Geology 3, 172–173.

Griffin, W.L., Ryan, C.G., Kaminsky, F.V., O'Reilly, S., Natapov, L.M., Win, T.T., Kinny, P.D., Llupin, I.P., 1999. The Siberian lithosphere traverse: mantle terranes and the assembly of the Siberian Craton. Tectonophysics 1–35.

Holtzman, B.K., Kohlstedt, D.L., Zimmerman, M.E., Heidelbach, F., Hiraga, T., Hustoft, J., 2003. Melt segregation and strain partitioning: implication for seismic anisotropy and mantle flow. Science 301, 1227–1230.

Ionov, D.A., Prikhodko, V.S., Bodinier, J.L., Sobolev, A.V., Weis, D., 2005. Lithospheric mantle beneath the south-eastern Siberian craton: petrology of peridotite xenoliths in basalts from the Tokinsky Stanovik. Contributions to Mineralogy and Petrology 149, 647–665.

Ionov, D., Chazot, G., Chauvel, C., Merlet, C., Bodinier, J.L., 2006. Trace element distribution in peridotite xenoliths from Tok, SE Siberian craton: a record of pervasive, multi-stage metasomatism in shallow refractory mantle. Geochimica et Cosmochimica Acta 70, 1231–1260.

Ionov, D.A., Doucet, L.S., Ashchepkov, I.V., 2010. Composition of the lithospheric mantle in the Siberian craton: new constraints from fresh peridotites in the Udachnaya-East kimberlite. Journal of Petrology 51, 2177–2210.
Jordan, T.H., 1975. The continental tectosphere. Reviews of Geophysics and Space Physics 13, 1–12.
Jung, H., Karato, S., 2001. Water-induced fabric transitions in olivine. Science 293, 1460–1463.
Kendall, J.M., Sol, S., Thomson, C.J., White, D.J., Asudeh, I., Snell, C.S., Sutherland, F.H., 2002. Seismic heterogeneity and anisotropy in the Superior Province, Canada: insights into the evolution of an Archaean craton. In: Fowler, C.M.R., Ebinger, C.J., Hawkesworth, C.J. (Eds.), The Early Earth: Physical Chemical and Biological Development. Geological Society, London, Special Publications, pp. 27–44.
Kinny, P.D., Griffin, B.L., Heaman, L.M., Brakhfogel, F.F., Spetsius, Z.V., 1997. SHRIMP U-Pb ages of perovskite from Yakutian kimberlites. Russian Geology and Geophysics 38, 97–105.
Kobussen, A.F., Christensen, N.I., Thybo, H., 2006. Constraints on seismic velocity anomalies beneath the Siberian craton from xenoliths and petrophysics. Tectonophysics 425, 123–135.
Kulakov, I.Y., 2008. Upper mantle structure beneath southern Siberia and Mongolia, from regional seismic tomography. Russian Geology and Geophysics 49, 187–196.
Li, Z., Chan, S.K., Garner, F.A., Bradt, R.C., 1995. Elastic stability of high dose neutron irradiated spinel. Journal of Nuclear Materials 219, 139–142.
Mainprice, D., 1990. A FORTRAN program to calculate seismic anisotropy from the lattice preferred orientation of minerals. Computer & Geosciences 16, 385–393.
Mainprice, D., Humbert, M., 1994. Methods of calculating petrophysical properties from lattice preferred orientation data. Surveys in Geophysics 15, 575–592.
Mainprice, D., Tommasi, A., Couvy, H., Cordier, P., Frost, D.J., 2005. Pressure sensitivity of olivine slip systems and seismic anisotropy of Earth's upper mantle. Nature 433, 731–733.
Mauler, A., Burlini, L., Kunze, K., Philippot, P., Burg, J.P., 2000. P-wave anisotropy in eclogites and relationship to the omphacite crystallographic fabric. Physics and Chemistry of the Earth 25, 119–126.
Mercier, J.-C.C., 1979. Peridotites xenolits and the dynamics of kimberlite intrusion. In: Boyd, F.R., Meyer, A. (Eds.), *The Mantle Sample: Inclusions in Kimberlites and Others Volcanics* Washington: AGU, pp. 197–212.
Michibayashi, K., Ina, T., Kanagawa, K., 2006. The effect of dynamic recrystallization on olivine fabric and seismic anisotropy: insight from a ductile shear zone, Oman ophiolite. Earth and Planetary Science Letters 244, 695–708.
Michibayashi, K., Tasaka, M., Ohara, Y., Ishii, T., Okamoto, A., Fryer, P., 2007. Variable microstructure of peridotite samples from the southern Mariana Trench: evidence of a complex tectonic evolution. Tectonophysics 444, 111–118.
Nickel, K.G., Green, D.H., 1985. Empirical geothermobarometry for garnet peridotites and implications for the nature of the lithosphere, kimberlites and diamonds. Earth and Planetary Science Letters 73, 158–170.
Nicolas, A., Poirier, J.P., 1976. Crystalline Plasticity and Solid State Flow in Metamorphic Rocks. Wiley, New York.
Nielsen, L., Thybo, H., Solodinov, L., 1999. Seismic tomographic inversion of Russian PNE data along profile Kraton. Geophysical Research Letters 26, 3413–3416.
Nielsen, L., Thybo, H., Egorkin, A.V., 2002. Implication of seismic scattering below the 8° discontinuity along PNE profile Kraton. Tectonophysics 358, 135–150.
Oreshin, S., Vinnik, L., Makeyeva, L., Kosarev, G., Kind, R., Wentzel, F., 2002. Combined analysis of SKS splitting and regional P traveltimes in Siberia. Geophysical Journal International 151, 393–402.
Pavlenkova, G.A., Pavlenkova, N.I., 2006. Upper mantle structure of the Northern Eurasia from peaceful nuclear explosion data. Tectonophysics 416, 33–52.
Pearson, D.G., Wittig, N., 2008. Formation of Archaean continental lithosphere and its diamonds: the root of the problem. Journal of the Geological Society of London 165, 895–914.
Pollack, H.N., Chapman, D.S., 1977. On the regional variation of heat flow, geotherms and lithospheric thickness. Tectonophysics 39, 279–296.
Priestley, K., Debayle, E., McKenzie, D., Pilidou, S., 2006. Upper mantle structure of eastern Asia from multimode surface waveform tomography. Journal of Geophysical Research B10304 10310.11029/12005JB004082.
Rosen, O.M., Condie, K.C., Natapov, L.M., Nozhkin, A.D., 1994. Archean and Early Proterozoic evolution of the Siberian Craton: preliminary assessment. In: K., C. (Ed.), Archean Crustal Evolution. Elsevier Sci, New York, pp. 411–459.
Rudnick, R.L., Nyblade, A.A., 1999. The thickness and heat production of Archean lithosphere: constraints from xenolith thermobarometry and surface heat flow. In: Fei, Y., Bertka, C.M., Mysen, B.O. (Eds.), Mantle Petrology: Field Observations and High-Pressure Experimentation. Spec. Publ. Geochem. Soc, Houston, pp. 3–12.
Schmidt, N.H., Olesen, N.Ø., 1989. Computer-aided determination of crystal-lattice orientation from electron-channeling patterns in the SEM. Canadian Mineralogist 27, 15–22.
Sobolev, N.V., 1990. Deep seated magmatism and evolution of lithosphere of the Siberian Platform. *Guide book, international field seminar*: Inst. Geol and Geophys, Sib Russ Acad Sci 1–20.
Sobolev, N.V., Logvinova, A.M., Zedgenizov, D.A., Pokhilenko, N.P., Malygina, E.V., Kuzmin, D.V., Sobolev, A.V., 2009. Petrogenetic significance of minor elements in olivines from diamonds and peridotite xenoliths from kimberlites of Yakutia. Lithos 112, 701–713.
Suvorov, V.D., Melnik, E.A., Thybo, H., Perchuc, E., Parasotka, B.S., 2006. Seismic velocity model of the crust and uppermost mantle around the Mirnyi kimberlite field in Siberia. Tectonophysics 420, 49–73.
Tasaka, M., Michibayashi, K., Mainprice, D., 2008. B-type olivine fabrics developed in the fore-arc side of the mantle wedge along a subducting slab. Earth and Planetary Science Letters 272, 747–757.
Taylor, W.R., 1998. An experimental test of some geothermometer and geobarometer formulations for upper mantle peridotites with applications to the thermobarometry of fertile lherzolite and garnet websterite. Neus Jahrbuch fur Mineralogie 172, 381–408.
Tommasi, A., Tikoff, B., Vauchez, A., 1999. Upper mantle tectonics: three-dimensional deformation, olivine crystallographic fabrics and seismic properties. Earth and Planetary Science Letters 168, 173–186.
Tommasi, A., Godard, M., Coromina, G., Dautria, J.M., Barsczus, H., 2004. Seismic anisotropy and compositionally induced velocity anomalies in the lithosphere above mantle plumes: a petrological and microstructural study of mantle xenoliths from French Polynesia. Earth and Planetary Science Letters 227, 539–556.
Tommasi, A., Vauchez, A., Godard, M., Belley, F., 2006. Deformation and melt transport in a highly depleted peridotite massif from the Canadian Cordillera: implications to seismic anisotropy above subduction zones. Earth and Planetary Science Letters 252, 245–259.
Tommasi, A., Vauchez, A., Ionov, D.A., 2008. Deformation, static recrystallization, and reactive melt transport in shallow subcontinental mantle xenoliths (Tok Cenozoic volcanic field, SE Siberia). Earth and Planetary Science Letters 272, 65–77.
Uarov, V.F., 1981. Seismic peculiarities of the upper mantle of Western Yakutia. Geol. Geophys. 9, 120–124.
Vauchez, A., Garrido, C.J., 2001. Seismic properties of an asthenospherized lithospheric mantle: constraints from lattice preferred orientations in peridotite from the Ronda Massif. Earth and Planetary Science Letters 192, 235–249.
Vauchez, A., Dineur, F., Rudnick, R., 2005. Microstructure, texture and seismic anisotropy of the lithospheric mantle above a mantle plume: insights from the Labait volcano xenoliths (Tanzania). Earth and Planetary Science Letters 232, 295–314.
Vissers, R.L.M., Drury, M.R., Strating, E.H.H., Spiers, C.J., van der Wal, D., 1995. Mantle shear zones and their effect on lithosphere strength during continental breakup. Tectonophysics 249, 155–171.
Vonlanthen, P., Kunze, K., Burlini, L., Grobety, B., 2006. Seismic properties of the upper mantle beneath Lanzarote (Canary Islands): model predictions based on texture measurements by EBSD. Tectonophysics 428, 65–85.
Wang, Q., Ji, S., Salisbury, M.H., Xia, B., Pan, M., Xu, Z., 2005. Pressure dependence and anisotropy of P-wave velocities in ultrahigh-pressure metamorphic rocks from the Dabie–Sulu orogenic belt (China): implications for seismic properties of subducted slabs and origin of mantle reflections. Tectonophysics 398, 67–99.
Yegorkin, A.V., Pavlenkova, N.I., 1981. Studies of mantle structure of U.R.S.S. territory on long-range seismic profiles. Physics of the Earth and Planetary Interiors 25, 12–26.